Effect of Divider Wall Shape on the Flow Development and Heat Transfer Characteristics in a Two-Pass Duct

Arun Chand, Nishab Ali, and Andallib Tariq

Abstract This paper presents the flow patterns and heat transfer distribution across the bend region in a two-pass rectangular duct for an inlet turbulent flow regime ($Re = 6500$). The results are presented at various vertical and horizontal planes located at different positions across the bend along the flow progression. Two divider wall configurations (in-between two-pass of the duct) are studied, i.e., (1) sharp-corner turn and (2) smooth curved turn. It has been noticed that flow gets completely modified because of divider wall shape. The numerical results reveal that primary and secondary flow in turn regime displays combined features of a bend-induced, Dean-type circulation. The flow dynamics and local heat transfer vary significantly with different divider wall configurations. For the duct with a sharp divider wall, a pair of counter-rotating Dean vortices induce after 90° near the end-wall of bend region. In contrast, for the duct with a smooth curved divider wall, vortices pair is induced close to the divider wall and stretched across the entire width. The results show that Dean vortices play an important role in enhancing localized heat transfer across the bend regime. Interestingly, the duct with a sharp divider wall exhibits higher localized heat transfer, whereas the duct with a smooth, curved divider wall exhibits lower localized heat transfer but more uniform distribution.

1 Introduction

The two-pass channels connected by a 180° turn are encountered in various engineering devices such as heat exchangers, ventilation piping systems, intake manifolds of engines, and the interior channels of gas turbine blades. The fluid experiences a strong curvature/bend in its path, which changes the flow characteristics. Bend regions in internal cooling passageways are associated with significant heat transfer

A. Chand (✉) · N. Ali · A. Tariq
AVTAR (Aerodynamics Visualization and Thermal Analysis Research) Lab, Mechanical and Industrial Engineering Department, Indian Institute of Technology Roorkee, Roorkee 247667, India
e-mail: arun_c@me.iitr.ac.in

enhancement and a pressure drop penalty, which are directly related to flow characteristics at these turns. When fluid is passed through 180° turn, flow characteristics change due to the development of curvature-induced primary and secondary flows, thus making this an essential flow investigation problem [1–4]. Therefore, many researchers are motivated to investigate the flow features in curvature ducts, but the scope was limited to either sharp or smooth 180° turn configurations. A limited study is present on the effect of divider wall shape. Modern engineering requires higher heat transfer enhancement and lower pressure drops, demanding an optimum turn configuration. A thorough understanding of turbulent flow dynamics and its consequence on heat transfer at different turn configurations is required for this aerothermal problem and thus motivates the current study.

2 Literature Review and Objective

Wang and Chyu [2] investigated the flow behavior and heat transfer distribution in a two-pass square duct with various turn geometries. They reported flow separation and the formation of dean vortices at the bend region, which altered the flow behavior downstream in the second pass. The divider wall generated a swirl in the cross-plane flow downstream of the bend regime, increasing heat transfer, which is greatly influenced by turn geometry. Liou et al. [4] investigated the flow characteristics and the effect of divider wall thickness in a two-pass square duct with a sharp 180° bend using LDV. They observed flow separation as the mainstream flow detached from the sharp divider wall. Furthermore, increasing divider wall thickness shifts the separation region near the divider wall tip and decreases the average turbulent kinetic energy after the bend. Liou and Chen [5] investigated the secondary flow fields in the two-pass rectangular duct using laser Doppler velocimetry (LDV), with and without rotation. In the case of a stationary duct, they reported that flow behavior is affected up to 3 D_h before the turn and 11 D_h downstream of the turn. A small corner vortex along with a bigger recirculation zone near the divider wall is observed in the primary flow. A dean vortex is formed, which covers almost half of the cross-section in the secondary flow field. The size of the separation zone decreased by 75% with rotation compared to a stationary duct. Son et al. [6] investigated the flow dynamics in a two-pass square duct using Particle Image Velocimetry (PIV) experiments and correlated them with heat transfer enhancement. They reported that vortex characteristics and flow impingement behavior in both primary and secondary flows are strongly related to localized wall heat transfer at a sharp bend. Saha and Acharya [7] studied flow behavior and heat transfer with nine different bend geometries. Significant effects of bend geometries on the overall performance of the cooling channel were observed.

Erelli et al. [8] investigated different turn configurations in a two-pass square duct. They discovered that the flow behavior varies significantly with turn configurations and that a bend in a square duct induces secondary flow, which affects the local heat transfer distribution. Recently, Liu et al. [9] studied internal flow field characteristics in square channels with different turn geometries. Only primary flow results

in the horizontal plane were reported. Yan et al. [10] varied the divider wall inclination angles in a two-pass duct and numerically investigated their effects on heat transfer characteristics and flow structure. Heat transfer was enhanced in the bend and upstream region, but decreased downstream of the bend as the positive divider inclination angle increased. With a negative divider inclination angle, the opposite heat transfer characteristics were observed. Reddy et al. [11] investigated the thermo-hydraulic performance of a novel curved serpentine coil and reported a 19% better performance compared to the conventional flat serpentine coil due to the enhanced chaotic nature of secondary flows. Wang et al. [12] investigated the evolution of secondary vortex structures and pressure loss for magneto-hydrodynamic flow in a square channel with a transverse magnetic field. The flow dynamics are reported to have a significant impact on convective heat transport in fusion reactor blankets.

The preceding discussion provides an overview of the complexities and importance associated with the aerothermal characterization of the bend regime. Available research emphasizes the overall flow field on a two-pass cooling channel and its effect on the temperature field. However, limited information is presented near the bend regime, which thus motivates the current study. This work focuses on studying flow structures and their dynamics at the 180° turn with two different divider shapes (sharp and smooth) at the bend region. The investigation aims to present a holistic insight into primary and secondary flow development and its consequences on heat transfer. Numerical simulation results are presented for a turbulent inlet condition at a Reynolds number of 6500. The results are expressed in terms of mean velocities, streamlines, and flow structures over primary and secondary flow regimes. Numerical simulation results are experimentally validated using Liquid Crystal thermography (LCT) and Particle Image Velocimetry (PIV) measurements. Although PIV technique can obtain velocity measurements with a high spatial resolution and accuracy, investigating such complex geometries where many measurement planes are required to understand the flow phenomena is quite challenging.

3 Computational Details

3.1 Computation Geometry and Grid Generation

The schematic and details of the two-pass rectangular duct geometries are shown in Fig. 1a, b. The computational domain dimensions are same as the experimental setup used for PIV measurement. The duct consists of an inlet and outlet section of length L($=$ 1180 mm) and hydraulic diameter D_h($=$70.4 mm) on both passes of the duct. Constant heat flux is provided at the bottom wall of both duct passes. The turbulent flow profile was checked at plane P^1, which is at a section length of $12D_h$ from the inlet (Fig. 2). The uniform bend width W and clearance c were equal in both ducts. For the smooth divider wall duct, bend radius R_W was chosen to achieve a uniform bend width W ($=2R_W$) equal to that of the sharp divider wall. Hexahedral structured
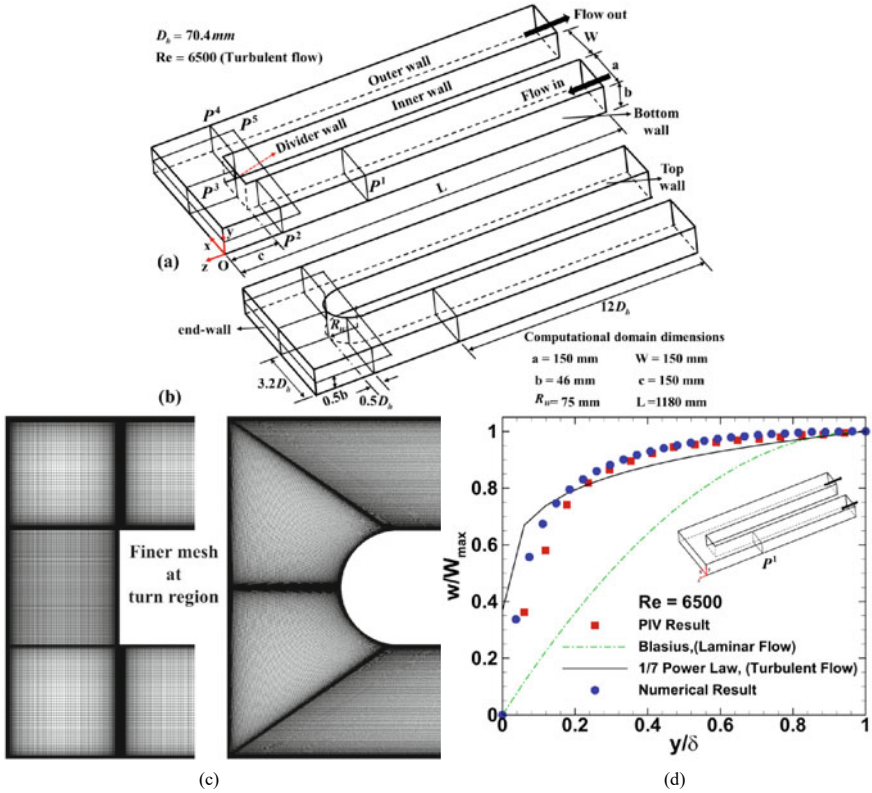
Fig. 1 Schematic diagram of computational domain with measurements planes (Two-pass duct with 180° bend) having **a** sharp divider wall, **b** smooth curved divider wall, **c** computational grid, **d** normalized inlet velocity profile at plane P^1

meshes were generated using ANSYS Meshing, where finer meshing is placed near the turn region, as shown in Fig. 2a. The turbulent flow was resolved using Realizable k-ε model with enhanced wall treatment, and a y$^+$ value of less than 1 was used for the first grid point near the wall. A total number of 7 million cells were used for the simulations.

3.2 Computational Setup and Boundary Conditions

The choice of a turbulence model is critical for turbulent flow involving three-dimensional flow phenomena, which demands accurate modelling. Numerous studies have demonstrated that the realizable k-ε turbulence model is capable of accurately predicting the flow structures and heat transfer distribution for flows involving strong adverse pressure gradients, recirculation, and separation, and it is widely used due

to its shorter computational time and accuracy [7, 8, 10]. Hence, steady state numerical simulations are performed using the realizable k-ε turbulence model present in Ansys Fluent (version 21R1) software with enhanced wall treatment. The working fluid used is air with constant physical properties and is assumed incompressible. The Reynolds number ($Re = 6500$) calculated from the experiments in a two-pass duct with a sharp divider wall was used in numerical simulation for both the duct geometry. A separate flow simulation without energy equation was performed in a $20D_h$ long rectangular duct having an exact cross-section as the present geometry. The fully developed turbulent velocity profile was extracted from the simulation, which was then used at the inlet of present computational domain. The solution methods and boundary conditions used in numerical simulations are shown in Table 1. The generalized form of steady Reynolds-averaged Navier–Stokes (RANS) along with energy equations are presented by Eq. 1–6 [13]:

$$\text{Continuity equation}: \frac{\partial}{\partial x_i}(\rho u_i) = 0 \tag{1}$$

$$\text{Momentum equation}: \frac{\partial}{\partial x_i}(\rho u_j u_i) = -\frac{\partial p}{\partial x_i} + \frac{\partial}{\partial x_j}\left[\mu\left(\frac{\partial u_i}{\partial x_j} + \frac{\partial u_j}{\partial x_i} - \frac{2}{3}\delta_{ij}\frac{\partial u_i}{\partial x_i}\right)\right]$$
$$+ \frac{\partial}{\partial x_j}(-\rho \overline{u'_i u'_j}) \tag{2}$$

$$\text{Energy equation}: \frac{\partial}{\partial x_i}(\rho u_i T) = \frac{\partial}{\partial x_j}\left[\left(\frac{\mu}{\Pr} + \frac{\mu_t}{\Pr_t}\right)\frac{\partial T}{\partial x_j} + u_i(\tau_{i_j})_{eff}\right] \tag{3}$$

where, $\left(-\rho\overline{u'_i u'_j}\right) = \mu_t\left(\frac{\partial u_i}{\partial x_j} + \frac{\partial u_j}{\partial x_i}\right) - \frac{2}{3}\left(\rho k + \mu_t\frac{\partial u_k}{\partial x_k}\right)\delta_{ij}$, and $\left(\tau_{ij}\right)_{eff} = \mu_{eff}\left(\frac{\partial u_i}{\partial x_j} + \frac{\partial u_j}{\partial x_i}\right) - \frac{2}{3}\left(\mu_{eff}\frac{\partial u_k}{\partial x}\right)\delta_{ij}$

$$\text{Turbulent kinetic energy (k)}: \nabla.\left(\rho k \bar{V}\right) = \nabla.\left[\left(\mu + \frac{\mu_t}{\sigma_k}\right)\nabla k\right]$$
$$+ G_k + G_b - \rho\varepsilon - Y_M + S_k \tag{4}$$

and turbulent dissipation rate (ε):

$$\nabla.\left(\rho\varepsilon\overline{V}\right) = \nabla.\left[\left(\mu + \frac{\mu_t}{\sigma_\varepsilon}\right)\nabla\varepsilon\right] + \rho C_1 S_\varepsilon - \rho C_2\frac{dy}{dx} \times \frac{\varepsilon^2}{k + \sqrt{\nu\varepsilon}}$$
$$+ C_{1\varepsilon}\frac{\varepsilon}{k}C_{3\varepsilon}G_b + S_\varepsilon \tag{5}$$

where: $C_1 = \max\left[0.43, \frac{\eta}{\eta+5}\right]$, $\eta = S\frac{k}{\varepsilon}$, $S = \sqrt{2S_{ij}S_{ij}}$ and model constants are $C_{1\varepsilon} = 1.44$, $C_2 = 1.9$, $\sigma_\varepsilon = 1.0$, $\sigma_k = 1.2$

Table 1 Boundary conditions and solution methods used in simulations

Boundary condition	Solution methods
Inlet: velocity inlet,	SIMPLE algorithm
Turbulent intensity 10%, and hydraulic diameter $D_h = 70.4$ mm	Second order discretization
Air inlet temperature 300 K	Second order upwind
Outlet: outflow	Convergence criteria of
Bottom wall: heat flux $q_w = 1000$ W/m^2	Flow equation: 10^{-6}
Other walls: adiabatic	Energy equation: 10^{-9}

3.3   Data Reduction

Numerical results in the form of velocity contours were presented at different vertical (xy & yz) and horizontal planes (zx). The vertical xy planes (P^2, P^4) are situated upstream and downstream of divider wall at a distance of 0.5D$_h$. At the same time, the vertical (yz) plane (P^3) is located at 3.2D$_h$, from the origin (Fig. 1). Further, primary flow in the horizontal (zx) plane is depicted using symmetry plane P^5. The temperature at bottom wall (T$_w$) and the local bulk air temperature (T$_{bulk}$) were obtained from the numerical solution. The heat transfer coefficient (h) and Nusselt number (*Nu*) distribution were then evaluated using Eqs. 6 and 7, respectively.

$$h \ = \ q_w \big/ (T_w \ - \ T_{bulk}) \tag{6}$$

$$Nu \ = h D_h \big/ K \tag{7}$$

3.4   Validation and Verification

Structured grids are generated using Ansys meshing and optimized using the grid independence test (Fig. 2a)
. The present mesh and turbulence model accurately captures flow physics and heat transfer distribution. The comparison of w/W$_{max}$ (W$_{max}$ is duct centerline velocity) at the plane *P^1* with PIV results, turbulent velocity profile (1/7th power-law) and laminar velocity profile (Blasius) reveals that the flow is completely turbulent for *Re* = 6500 as shown in Fig. 1d. Heat transfer results are validated against the experiment using LCT technique (Fig. 2b). The numerical simulation accurately captured the primary recirculation region near the divider wall, as observed from the PIV experiment (Fig. 3a, b). However, the presence of the recirculation zone is still visible near the corner area of the first pass, as shown in Fig. 3a.
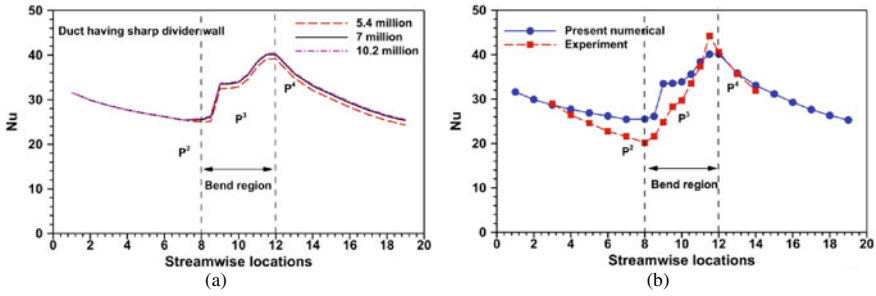
Fig. 2 Spanwise averaged *Nu* at various locations along the streamwise direction **a** at three different mesh sizes **b** for model validation
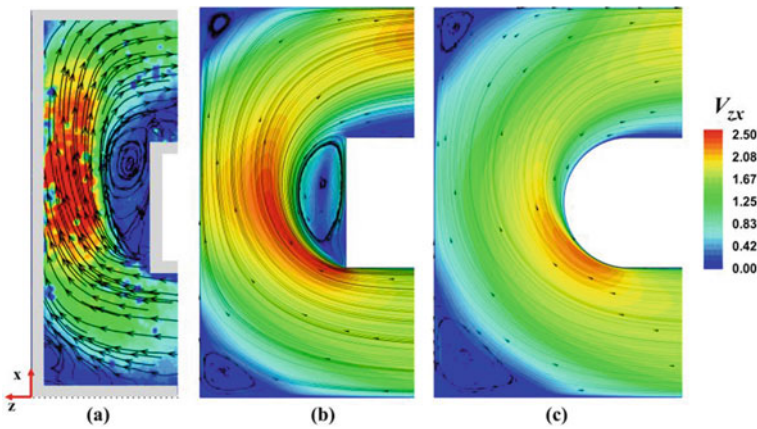

Fig. 3 Streamlined velocity profile of primary flow on horizontal plane P^5 **a** experimental (PIV) result, **b** numerical result with sharp divider wall, and **c** smooth curve divider wall

4 Results and Discussion

The primary and secondary flow progression is explained by velocity contour (V_{mag}) superposed with streamlines at the horizontal plane (P^5) and vertical planes (P^2–P^4) respectively. Finally, the relationship between flow progression and heat transfer has been discussed.

4.1 Flow Progression

The streamlined contour of velocity for the duct with a sharp divider wall is shown in Fig. 3b, and a total of four vortexes can be observed. The incoming flow is uniform and smooth in the first pass, and the flow deviates toward the inner wall just upstream

of the bend (P^2) due to the curvature in the bend section. As a result, a radial pressure gradient and a lower pressure zone are formed toward the inner wall of the first pass. Flow accelerates near the inner wall of the first pass and decelerates near the outer wall. The fluid along the outer wall of the first pass impinges on the end-wall of the bend region, forming the first recirculation zone in the duct at the bend corner of the first pass. Moreover, the flow is abruptly redirected by sharp edge of the divider wall. Along with pressure reduction, it causes flow separation and a primary recirculation zone (primary vortex) is formed at the tip of the divider wall, as shown in Fig. 3b. Further downstream, at the outer bend corner in the second pass, a third recirculation zone forms, similar to the first recirculation zone. The primary flow separation zone at the tip of the divider wall extends further downstream in the second pass.

Figure 3b shows the streamlined velocity contour for the duct with a smooth divider wall. The two small recirculation zones at the corners occur for the same reason as explained previously, but their size increases. The circular divider wall shape causes the upstream fluid to stick more easily to the inner wall, so flow remains strongly attached. This causes an enhanced radial pressure gradient in section (P^2), and flow is accelerated near the divider wall and decelerated at the outer wall of the first pass. The fluid close to the outer wall of the first pass impinges farther away on the end-wall of the bend region, forming a larger recirculation zone compared to the duct with a sharp divider wall. As shown in Fig. 3c, the circular divider wall reduces the primary recirculation zone in the bend area. The mainstream fluid follows the curved geometry, and this strong flow attachment leads to a negligible low-pressure zone near the tip of the divider wall. This flow attachment is further reflected downstream of the bend, with no recirculation zone at the inner wall of the second pass. Because there is no separation of primary flow in a duct with a smooth divider wall, the velocity contour is more uniform.

The primary flow observations in the bend region and past literature manifest secondary flow development and its consequences on heat transfer. The primary flow encounters a sharp bend, which causes centrifugal instability [14], resulting in the formation of a pair of counter-rotating vortices at plane P^3 (after 90° rotation of flow) known as the Dean vortex, as seen in Fig. 4. Vortex pair is noted by upper clockwise rotating vortices and lower anticlockwise rotating vortices. The development of vortices enhances the mixing between fluid layers due to the higher velocity gradients in the transverse direction. As shown in Fig. 4a, Dean vortices form away from the sharp divider wall in areas of mainstream flow (where centrifugal instability is induced). Low-velocity magnitude at plane P^3 confirms flow entrapment due to the primary recirculation zone as well as the absence of centrifugal instabilities. Hence, Dean vortices are not induced near the tip of the divider wall. The Dean vortex pair propagates upwards and outwards as the flow advances downstream (180° turn) due to centrifugal forces pushing the main flow outward.

Dean vortices develop near the tip of the smooth divider wall in the region of mainstream flow, as seen in Fig. 4b. Also, the effect of dean vortices extends the entire plane width, reflecting the uniform flow distribution observed in primary flow. Further, the uniform velocity contours are present at vertical planes compared to the duct with a sharp divider wall, and this trend continues downstream the bend in
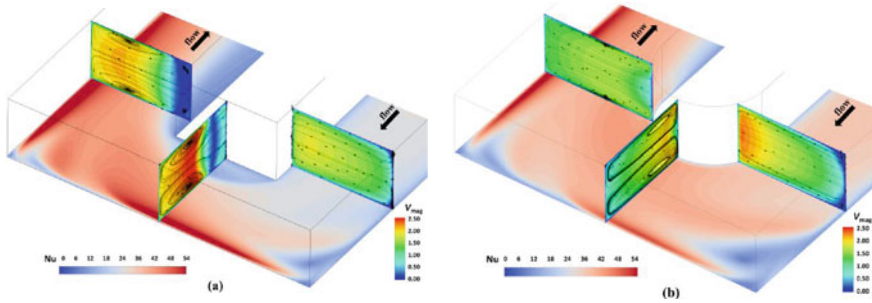
Fig. 4 Flow progression (P^2-P^4) with surface Nusselt number (at bottom wall) distribution across 180° bend having **a** sharp divider wall **b** smooth curve divider wall

the second pass of the duct. Dean vortices develop in mainstream flow, as observed for both geometries, implying that centrifugal instabilities are essential for their development.

4.2 Heat Transfer

The surface heat transfer distribution near the bend region strongly correlates with primary and secondary flows. Upstream of the bend regime with the sharp divider wall, *Nu* values are low due to the boundary layer formation caused by the long entry length of the first pass, which inhibits heat transfer between the surface and the heated air stream. However, there is a significant increase in *Nu* values in the bend regime, particularly in the region of mainstream flow (Fig. 4a). The *Nu* values were observed to be successfully augmented from an order of 20–25 to an order of 50. Although primary flow enhances the heat transfer, the impingement region of dean vortices has slightly higher *Nu* values. The secondary flow induces huge turbulence with high-velocity gradients locally, resulting in higher fluid mixing and momentum transfer between fluid layers. The mixing/momentum transfer mechanism helps in intense augmentation of heat transfer that is reflected by the higher values of local *Nu* nearby the dean vortex. In contrast, heat transfer is lower on the inner side of the bend near the sharp divider wall. It is possibly due to flow entrapment resulting from flow separation by this sharp edge divider. The comparatively uniform primary flow and stretched secondary flow pattern in duct with a smooth curved divider wall results in uniform *Nu* distribution across the bend regime as seen in Fig. 4b.

Now the surface *Nu* at plane *P³* with flow structure is closely presented in Fig. 5. Interestingly for the duct with a sharp divider wall (Fig. 5a), *Nu* is very low in the regime of separated flow (recirculation flow) where flow entrapment takes place. But in the regime of Dean vortices, very intense enhancement in surface *Nu* is observed. *Nu* value on the extent of the separated region is found to be an order of 20, which is intensely raised to approx. 35 (i.e., 1.5 times) on the extent, where Dean vortices
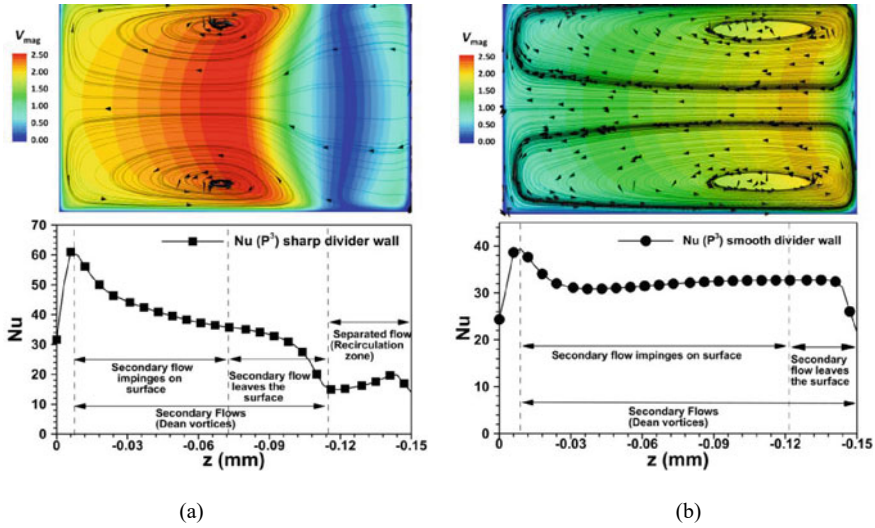
Fig. 5 Effect of secondary flow structure on surface Nusselt number distribution at vertical plane P^3 for: **a** duct with sharp divider wall and **b** duct with smooth curve divider wall

leave the surface. Subsequently, a further increment is seen in *Nu,* approx. up to 60 at the extent where Dean vortices impinge the surface. Therefore, the surface impingement effect is more pronounced in heat transfer enhancement as compared with the surface leaving effect of Dean vortices. The possible reason is that surface impingement is more significant in breaking the boundary layer than the surface leaving effect. As shown in Fig. 5b, the *Nu* distribution is uniform for the duct with a curved divider wall. The only exception to a higher *Nu* value is the region where the local impinging jet effect of dean vortex is present.

5   Conclusion

The investigation presents detailed flow dynamics and heat transfer behavior across a bend regime in a two-pass rectangular duct with two different divider wall shapes. The divider wall configurations studied are, i.e., the sharp divider wall and the smooth divider wall for an inlet turbulent flow regime. The shape of a divider wall completely changes the flow behavior in the bend region. For the duct with a sharp divider wall, a primary separation bubble is formed near the divider wall, whereas flow remains attached to the curved divider wall. The primary flow significantly affects secondary flow development, modifying the flow pattern and propagation. The secondary flow structure, in the form of counter-rotating Dean vortices, is observed on the transverse plane as the flow turns 90° and propagates in the direction of flow advancement. As observed for both geometries, Dean vortices develop in mainstream flow at the bend

regime where centrifugal instabilities exist, implying that centrifugal instabilities are critical for their development. A strong correlation is found between these vortex structures and heat transfer behavior at the bend. An enhancement in localized heat transfer is observed in the regime of Dean vortices due to impinging jet-like effect. The surface averaged Nusselt number is found to be more uniform in the duct with a smooth divider wall. It can be confirmed that the divider wall shape affects the mainstream (primary) flow, which in turn affects the secondary flow magnitude in transverse direction (vertical planes).

References

1. Azzola J, Humphrey JAC, Iacovides H, Launder BE (1986) J Fluids Eng Trans ASME 108:214
2. Wang TS, Chyu MK (1994) J Thermophys Heat Transf 8:595
3. Schabacker J, Bolcs A, Johnson BV (1998) Am Soc Mech Eng 1
4. Liou TM, Tzeng YY, Chen CC (1998) Proc ASME Turbo Expo 4
5. Liou TM, Chen CC (1997) Proc. ASME Turbo Expo 3:167
6. Son SY, Kihm KD, Han JC (2002) Int J Heat Mass Transf 45:4809
7. Saha K, Acharya S (2012) J Turbomach 135
8. Erelli R, Saha AK, Panigrahi PK (2015) Int J Heat Mass Transf 89:667
9. Liu R, Li H, You R, Tao Z (2020) AIP Adv 10
10. Yan H, Luo L, Du W, Wang S, Sunden B, Huang D (2021) Int J Therm Sci 166:106969
11. Reddy DS, Khan MK, Awasthi K (2020) Phys Fluids 32
12. Wang H, Ni MJ, Zhang NM (2022) Phys Fluids 34
13. ANSYS, Inc. (2021) ANSYS Fluent User's Guide, Release 21R1
14. Ali N, Tariq A (2023) Phys Fluids 35:015110